# Achieving depth resolution with gradient array survey data through transient electromagnetic inversion

*Patrick Belliveau, Eldad Haber, University of British Columbia*


## SUMMARY

We apply state of the art 3D transient electromagnetic simulation and inversion techniques to a single transmitter gradient array survey. Direct current (DC) gradient array surveys offer a simple way to map horizontal variations in subsurface conductivity but suffer from a lack of depth resolution. We demonstrate by numerical experiment that it is possible to recover useful depth information from gradient array surveys. This is achieved by inverting the early off-time transient voltage decay along with the DC data—data that is often already collected in the case of an induced polarization survey.


## INTRODUCTION

A gradient array survey is a grounded source electromagnetic survey in which direct current (DC) is injected into a long line source transmitter and data is collected by electric dipole receivers far from the transmitter electrodes. Such surveys are an efficient way to map horizontal variations in subsurface conductivity but they are known to be quite poor at resolving the depth of anomalies (see e.g. Zonge et al., 2005).

Gradient arrays are used to collect induced polarization (IP) as well as DC data. In a time-domain IP survey, DC data is recorded and then the transmitter current abruptly shut off. The transient decay of the receiver voltages is then measured. In interpreting IP data, it is generally assumed that any effects of electromagnetic induction will be negligible for the time windows used to generate the IP data. Quantitative interpretation of IP parameters requires a model of subsurface conductivity, which is normally built from interpretation of DC data alone. However, there may be much information in the transient decay data that can be used to develop a better conductivity model. The long source wires used in gradient array surveys create significant electromagnetic induction. Measuring the signal from these induced currents removes the potential field nature of DC gradient array data, with the shape of the transient decay curve offering a great deal of information about the conductivity and depth of anomalies.

In this work, we compare DC and transient electromagnetic inversions of synthetic gradient array data. We are only aware of one published instance of transient electromagnetic inversion being applied to DC or IP survey data. Kang and Oldenburg (2015) inverted early-time IP decay data using electromagnetic techniques in an attempt to tackle the IP electromagnetic coupling problem.

We describe the electromagnetic forward modelling and inversion techniques used to carry out our numerical experiment and then compare our results to standard DC inversion.

## FORWARD MODELLING

Grounded source electromagnetic surveys are governed by the quasi-static time-domain Maxwell equations. Ignoring IP effects, the equations are

$$\begin{aligned} \nabla \times \mathbf{e} &= -\frac{\partial \mathbf{b}}{\partial t} \\ \nabla \times \mu^{-1}\mathbf{b} - \sigma \mathbf{e} &= \mathbf{j}^s, \end{aligned} \tag{1}$$

where $\mathbf{e}$ is the electric field, $\mathbf{b}$ is the magnetic flux density, $\mathbf{j}^s$ is the source current, $\sigma$ is the electrical conductivity, and $\mu$ is magnetic permeability. We consider the equations in a bounded cuboidal domain $\Omega$ on the time interval $[0,t]$. We use the boundary condition $\mathbf{b} \times \hat{\mathbf{n}} = \mathbf{0}$ on $\partial\Omega$. We assume that at $t = 0$ the transmitter will have been switched on long enough to achieve a DC steady state. Then the current is abruptly shutoff and the transient receiver voltage decay is measured.

The DC resistivity equation forms the initial condition for our transient electromagnetic modelling. Formulated in terms of electric potential $\phi$, it reads

$$\nabla \cdot \sigma \nabla \phi = -\nabla \cdot \mathbf{j}^s. \tag{2}$$

The initial electric field is $\mathbf{e}_0 = -\nabla\phi$ and the initial magnetic flux density is zero.

### Discretization

We discretize equations (1) using a method of lines approach. Spatial operators are discretized using a finite volume method on an OcTree mesh, as previously described by Haber and Heldmann (2007). We also discretize the DC problem used to compute the initial electric field on the same OcTree mesh as used for modelling the transient fields. We solve a discretized version of equation (2) and computed the initial electric field by taking the negative gradient of the potential numerically.

Maxwell's equations in time are known to be very stiff in the quasi-static regime (e.g. Haber et al., 2004), making their time integration a difficult problem. One must use very small time-steps to insure stability if using an explicit time-stepping scheme (e.g. Commer and Newman, 2004). An alternative is to use implicit methods. In previous work, such as Haber et al. (2004), we have used backward Euler time-stepping due to its simplicity and excellent stability properties. In this work we use the second order backward difference formula (BDF-2) time-stepping scheme. It retains most of the stability of backward Euler while offering improved accuracy, allowing for the use of larger time-steps.

After discretizing equations (1) in space and time they are rearranged to eliminate explicit dependence on $\mathbf{b}$. This gives the following system of equations that must be solved at each

time-step to update the electric field:

$$\left(\mathbf{C}^T\mathbf{M}^f_{\mu^{-1}}\mathbf{C}+\frac{3}{2}\delta_t^{-1}\mathbf{M}^e_\sigma\right)\tilde{\mathbf{e}}_{n+1}= \frac{3}{2}\delta_t^{-1}\left(\tilde{\mathbf{q}}_{n+1}-\frac{4}{3}\tilde{\mathbf{q}}_n+\frac{1}{3}\tilde{\mathbf{q}}_{n-1}-\mathbf{M}^e_\sigma(\frac{4}{3}\tilde{\mathbf{e}}_n-\frac{1}{3}\tilde{\mathbf{e}}_{n-1})\right), \quad (3)$$

where $\mathbf{C}$ is the self-adjoint discretization of the curl operator and $\mathbf{M}^f_\mu$ and $\mathbf{M}^e_\sigma$ are mass matrices. The vectors $\tilde{\mathbf{e}}$ and $\tilde{\mathbf{b}}$ are the discrete electric field and magnetic flux density on the OcTree mesh. The source term $\tilde{\mathbf{q}}$ is computed by approximating transmitter wirepath on the edges of the OcTree mesh cells. Each BDF-2 time-step requires the electric field at the previous two time steps. Thus, the initial time-step must be taken using a different method. We take the first time-step using the backward Euler method.

## INVERSION ALGORITHM

We formulate the inverse problem as a regularized least-squares optimization problem. We seek the conductivity model $\mathbf{m}$ that minimizes the unconstrained objective function

$$\Phi=\left\|\mathbf{PA}(\mathbf{m})^{-1}\mathbf{q}-\mathbf{d}\right\|^2_{W_d}+\beta\left\|\mathbf{W}_m(\mathbf{m}-\mathbf{m}_{\text{ref}})\right\|^2. \quad (4)$$

The first term represents the data misfit, computed by taking the weighted two-norm of the data residual. $\mathbf{A}$ is the forward modelling operator, $\mathbf{P}$ is a measurement operator that computes the predicted data from the electric field and $\mathbf{d}$ is the observed data. Use of the $W_d$ norm indicates that the misfit is weighted by the inverse standard deviations of the data. The second term is the regularization operator which penalizes model roughness relative to a reference model $\mathbf{m}_{\text{ref}}$. We minimize equation (4) using a projected Gauss-Newton method. The computed model is strongly dependent on the value of the tradeoff parameter $\beta$. We gradually adjust beta throughout the course of the inversion using an iterated Tikhonov procedure, described in Haber et al (2007).

## SYNTHETIC EXAMPLE

We simulated gradient array style data over a simple block in a half-space model. The test model consisted of a 200 m × 200 m × 125 m block of conductivity 3 S/m buried at a depth of 75 m in a 0.01 S/m halfspace. The survey layout is shown in figure 1. The transmitter is 2 km long, with the target block centered along the length of the transmitter. Receiver electrodes were placed in a grid layout over an 800 m × 800 m area with 50 m spacing between each electrode in both the x and y directions. This made for a total of 289 50 m electric dipole receivers.

This core area of interest was meshed by a grid of 50 m X 50 m X 25 m cells covering a 1200 m X 1200 m area centered on the anomalous block and extending to a depth of 600 m. The domain was then extended into the air and padded to a distance of 25 km from the domain center in all directions.

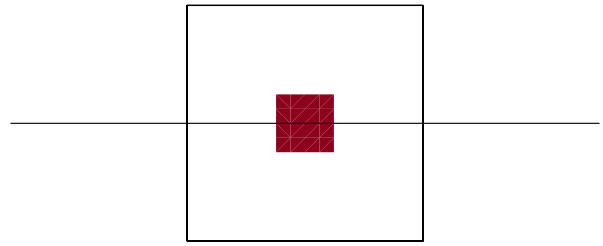

Figure 1: Synthetic model with conductive block shown in red. Black line shows transmitter. The black rectangle shows the extent of the receiver grid.

### DC inversion

We first simulated a DC survey using the above described earth model and survey configuration. The DC data consists of the x-component (along the direction of the transmitter axis) of the electric field integrated over each receiver dipole, giving the receiver voltage. The data generated from our synthetic model is plotted in figure 2. The conductive block shows up in the data as a discernible anomaly well above the noise level.

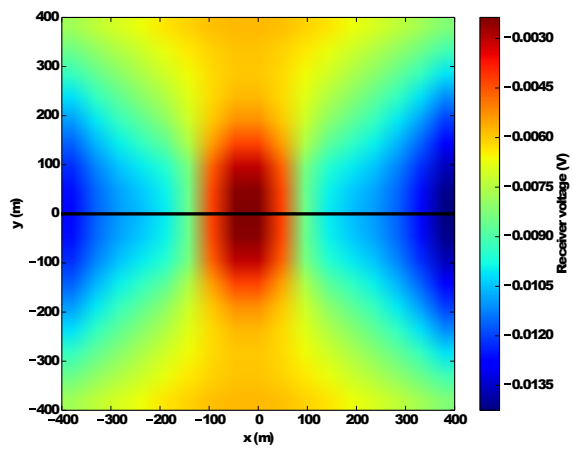


Figure 2: DC data, with section of transmitter shown as black line.

Independent gaussian noise was added to each datum, with standard deviation 3% of the datum value. The data were then inverted using a 0.01 S/m halfspace (correct background) as both initial and reference model. Standard deviation of each datum was set to 3% of its value. The inversion converged to the desired misfit after just 4 Gauss-Newton iterations with a fixed regularization parameter. The resulting conductivity model is shown in figure 3.

Although the inversion converged quickly the recovered model is rather unsatisfactory. We see that the conductivity is not well constrained by the data. The inversion vastly underestimates the conductivity of the anomaly and moves it to the surface. The anomaly being pushed to the surface by the inversion is the expected behaviour. The DC electric potential is a potential field and we energize it only from a single source. Our results clearly indicate the well-known lack of depth resolution in DC

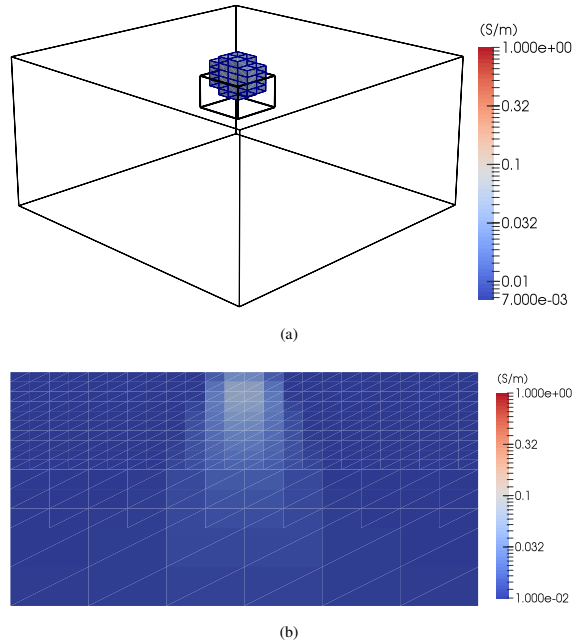


Figure 3: a) recovered model, showing all cells with conductivity above 0.03 S/m. b) depth section of recovered model in the x-z plane at $y = 0$.

gradient array surveys.

This problem might be lessened by the use of a depth weighting procedure but this is not a guaranteed solution and it adds further bias to the inversion results. Using transient decay data allows anomaly depth to be constrained by the data itself.

**Transient EM inversion**

Transient decay data were simulated at a series of 20 roughly logarithmically spaced time-steps from $1.6 \times 10^{-}4$ s to $7.8 \times 10^{-}3$ s. Voltages for those times are shown in figure 4.

The conductive block creates a strong anomaly at both times. At $1.6 \times 10^{-}4$ s the background response is dominated by induced current spreading from the transmitter wire. In other words, we see strong EM coupling. Still, the conductive anomaly creates a strong low in the electric field. By $7.8 \times 10^{-}3$ s, the size of the anomaly has greatly decreased relative to the background, as the induced currents from the wire have dissipated.

The transient data were inverted along with the DC data, starting from the same initial and reference models as for the DC inversion in the previous section. The inversion converged after seven iterations, with the value of the tradeoff parameter decreased after the first four iterations. The resulting model is shown in figure 5.

The recovered model has spurious lobes of conductivity slightly above background value descending to depth but the main body of the anomaly is recovered at the correct depth. The top of the the anomaly is recovered very well, with a maximum recovered conductivity of 4.1 S/m but the depth extent of the block is poorly resolved. The inversion recovers a thin body relative

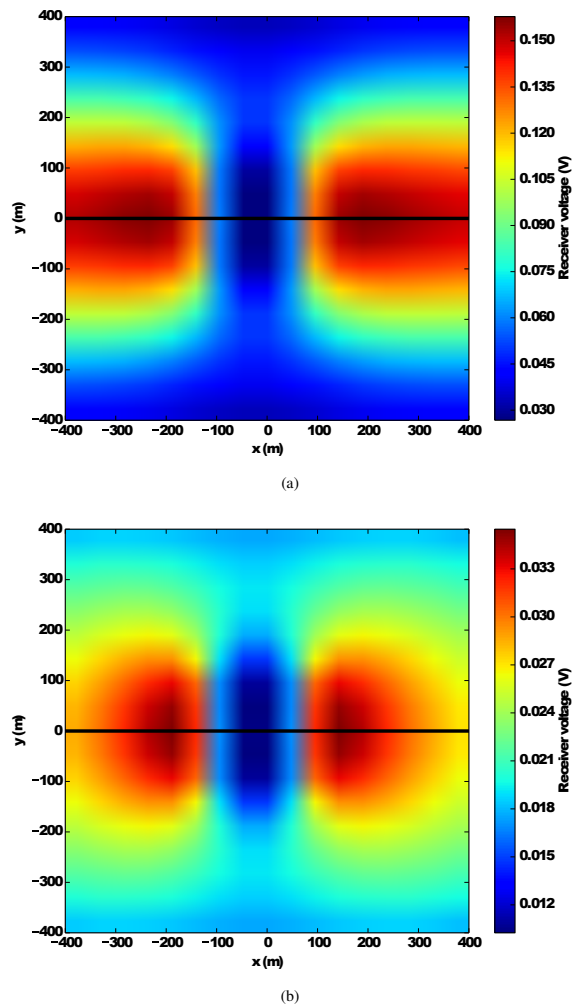


Figure 4: Transient voltage data a) at $1.6 \times 10^{-4}$ s. b) at 0.0048 s

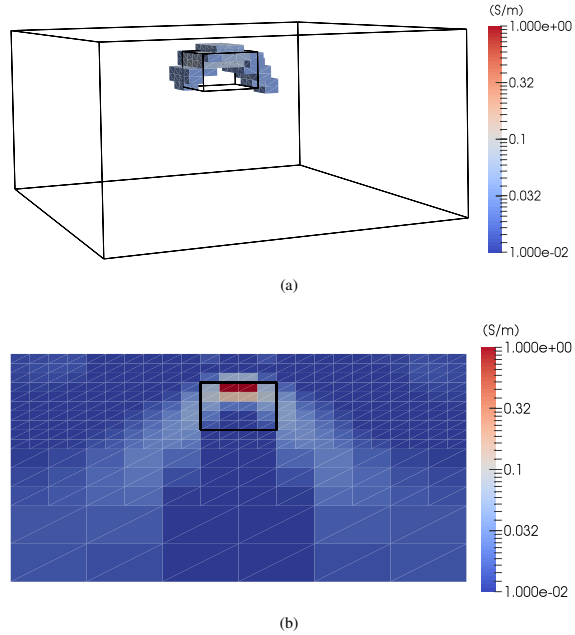


Figure 5: a) recovered model, showing all cells with conductivity above 0.03 S/m. b) depth section of recovered model in the x-z plane at $y = 0$.

to the true conductive block. This result is still sub-optimal but it clearly represents a large improvement from the DC case.

## FUTURE WORK

This abstract shows promising early results but the technique described requires further investigation with synthetic data to test its limits and then subsequent application to field data. Our algorithms are embedded in a strong computational framework that can be applied to inversions of much larger datasets over wider areas.

**EDITED REFERENCES**

Note: This reference list is a copyedited version of the reference list submitted by the author. Reference lists for the 2016 SEG Technical Program Expanded Abstracts have been copyedited so that references provided with the online metadata for each paper will achieve a high degree of linking to cited sources that appear on the Web.

**REFERENCES**

Haber, E., U. Ascher, and D. Oldenburg, 2000, On optimization techniques for solving nonlinear inverse problems: Inverse problems, **16**, 1263–1280, http://dx.doi.org/10.1088/0266-5611/16/5/309.

Haber, E., U. Ascher, and D. Oldenburg, 2004, Inversion of 3D electromagnetic data in frequency and time domain using an inexact all-at-once approach: Geophysics, **69**, 1216–1228, http://dx.doi.org/10.1190/1.1801938.

Haber, E., D., Oldenburg, and R. Shektman, 2007, Inversion of time domain three-dimensional electromagnetic data: Geophysical Journal international, 171, 550–564, http://dx.doi.org/10.1111/j.1365-246X.2007.03365.x.

Kang, S., and D. W. Oldenburg, 2015, Recovering IP information in airborne-time domain electromagnetic data: ASEG Extended Abstracts 2015: 24th International Geophysical Conference and Exhibition, 1–4, http://dx.doi.org/10.1071/ASEG2015ab102

Zonge, K., J. Wynn, and J. Urquhart, 2005, Resistivity, induced polarization, and complex resistivity, in Near Surface Geophysics, D. K. Butler, ed.: SEG, 265–300.